

Molecular Recognition in Asymmetric Counteranion Catalysis: Understanding Chiral Phosphate-Mediated Desymmetrization.

Fernanda Duarte^{a*} and Robert S. Paton^{b*}

^aEaStCHEM School of Chemistry, University of Edinburgh, Joseph Black Building, David Brewster Road, Edinburgh EH9 3FJ, U.K. ^bChemistry Research Laboratory, University of Oxford, Mansfield Road, Oxford OX1 3TA, U.K.

KEYWORDS: *ion-pairing, asymmetric organocatalysis, desymmetrization, meso-aziridinium, meso-episulfonium, molecular dynamics, density functional theory.*

ABSTRACT: We describe the first theoretical study of a landmark example of chiral anion phase transfer catalysis: the enantioselective ring-opening of meso-aziridinium and episulfonium cations promoted by asymmetric counteranion-directed catalysis (ACDC). The mechanism of ion-pairing, ring-opening and catalyst deactivation have been studied in the condensed-phase with both classical and quantum methods using explicitly and implicitly solvated models. We find that the stability of chiral ion-pairs, a pre-requisite for asymmetric catalysis, is dominated by electrostatic interactions at long-range and by CH...O interactions at short-range. The decisive role of solvent upon ion-pair formation and of non-bonding interactions upon enantioselectivity are quantified by complementary computational approaches. The major enantiomer is favored by a smaller distortion of the substrate, demonstrated by a distortion/interaction analysis. Our computational results rationalize the stereoselectivity for several experimental results and demonstrate a combined classical/quantum approach to perform realistic-modelling of chiral counterion catalysis in solution.

INTRODUCTION

The formation of ion-pairs with a charged, chiral catalyst has emerged as a versatile strategy for the asymmetric catalysis of reactions proceeding via charged intermediates.¹⁻⁴ The formation of a contact ion-pair between oppositely charged catalyst and substrate/intermediate provides a chiral environment in which an enantioselective reaction may then occur. Despite a rich history of asymmetric ion-pairing catalysts in synthesis, such as in phase-transfer catalysis, this work focused mostly on using chiral *cations*; the development of chiral *anions* as catalysts is a much more recent phenomenon. The induction of enantioselectivity in a reaction proceeding through a cationic intermediate by means of ion pairing with a chiral, enantiomerically pure anion provided by the catalyst, has been termed Asymmetric Counteranion-Directed Catalysis (ACDC).⁴ This definition encompasses both ion-pairs clearly stabilized by hydrogen bonds (which can include asymmetric Brønsted acid catalysis) and those for which the cationic intermediate lacks the ability to form hydrogen bonds, as demonstrated by List in 2006.^{4,5} The conjugate bases of axially chiral phosphoric acids (CPAs) have since been used with considerable success in a wide range of such transformations, including the allylic substitution/electrocyclization of a protonated o-quinone methide,⁶ aldol,⁷ and Mannich reactions,⁸ among others.

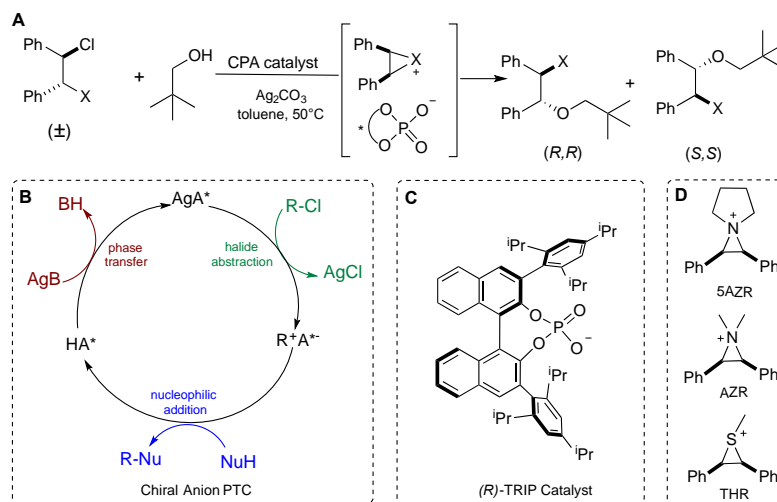
For a comprehensive coverage of the reaction catalyzed by CPAs see ref 9.

Identifying the occurrence of chiral counterion catalysis can be challenging, or even controversial, when alternative activation modes, such as hydrogen-bonding (HB) rather than electrostatic ion-pairing, can occur. In these cases the extent of proton transfer governs whether chirality is induced by purely ion-pairing or HB interactions.^{10,11} Experimental studies of Brønsted acidic activation of imine/carbonyl electrophiles suggest these reactions proceed *via* proton-transfer leading to substrate:catalyst ion-pairs. However, the NMR studies of Gschwind and Rueping present a nuanced picture, in which the nature of the imine substituents as well as temperature, solvent, and catalyst acidity all influence the extent of HB vs. ion-pairing. HB is favored at room temperature and by less-basic imines, while ion-pairing prevails at lower temperatures or with more basic imines.¹⁰ Recent dielectric spectroscopy and NMR experiments by Rueping and Hunger confirm the presence of ion-paired complexes.¹¹ The predominantly ionic character of these complexes has also been recently discussed by Gschwind.^{12,13} These results pose a challenge for routinely-used computational models, since gas-phase calculations disfavor the formation of charge-separated species, while the use of implicit solvation models neglects specific solute-solvent interactions.

Toste and co-workers first applied chiral counteranions in asymmetric phase-transfer catalysis (PTC).¹⁴ The chiral anion, the conjugate base of a CPA, extracts a cationic reagent from the aqueous or solid phase to form a contact ion-pair that promotes an asymmetric reaction. This strategy was applied to the asymmetric synthesis of β -alkoxy amines via the desymmetrization of an achiral re-

active intermediate (**Scheme 1**). Extraction of Ag^{I} from solid Ag_2CO_3 to the liquid phase produces a silver phosphate, which following chloride abstraction from a β -chloro tertiary amine generates an aziridinium:phosphate ion-pair (and insoluble AgCl). This was extended to the

Scheme 1. (A) Desymmetrization of a *meso*-cation by chiral phosphate-directed PTC; (B) Proposed catalytic cycle for this strategy; (C) Chiral phosphate counteranion used; (D) Cationic intermediates analyzed in this work. X = aziridinium or episulfonium substitution, B = basic anion, A* = chiral anion.

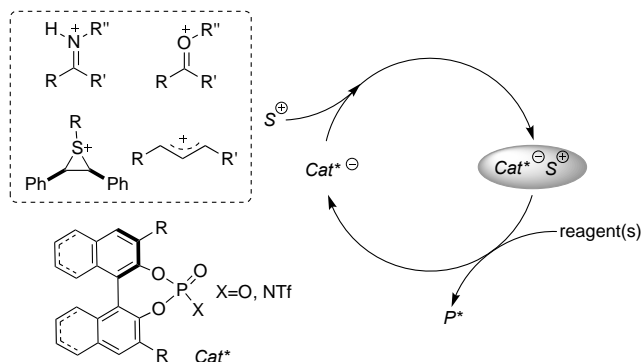


desymmetrization of *meso*-episulfonium ions generated by protonation of the leaving group trichloroacetimidates. The counteranion provides a chiral environment in which the electrophile undergoes ring opening by an alcohol nucleophile to form either of the enantiomeric (R,R) or (S,S) products, with deprotonation by the phosphate closing the catalytic cycle. Using the 3,3'-bis(2,4,6-triisopropylphenyl)-1,1'-binaphthyl-2,2'-diylphosphate (TRIP) anion, the reaction is highly enantioselective (90–99 % ee) over a range of 1°, 2° and 3° alcohols.¹⁵

Goodman and Simón,^{16,17} Himo,^{18,19} and others^{7,20,21} have pioneered the computational study of BINOL-phosphoric acid-catalyzed reactions of imines. For these systems, a bifunctional mode of action has been established, in which the catalyst's acidic proton activates the imine electrophile through a hydrogen bond, while the P=O bond simultaneously coordinates to an acidic X-H bond (X = N, O, S) of the nucleophilic reagent. This two-point binding mode has been used extensively to understand and predict selectivity across a wide range of reactions using CPA catalysts^{9,22} and the related bis-iminophosphoranes.^{23–25} However, a similar level of understanding about how these catalysts impart enantioselectivity in anionic form, for substrates incapable of forming hydrogen bonds, is currently lacking.

Chiral anions including phosphates, phosphoramides, sulfonimides and borates² play an increasingly important role in asymmetric catalysis (**Scheme 2**), however, significant questions remain regarding their mode of action and the nature of molecular recognition.²⁶ The structures of contact ion-pairs formed between chiral catalyst and sub-

strate in the absence of strongly-directional H-bonding interactions are less well understood when compared to neutral reactions. The directionality of the electrostatic attraction in ion-pairs, which is dominated by the isotropic charge-charge interaction, is weak and the distance dependence less dramatic than e.g. hydrogen-bonding or dispersion interactions.²⁷ Quantum chemical approaches to rationalize and predict stereoselectivity have been well described,^{28–32} but the ability of routine approximations such as implicit solvation models to accurately describe ion-pairing in solution remains an open question. These questions are addressed by this work. For Toste's landmark anionic asymmetric PTC reaction (**Scheme 1**) we investigate the structures, dynamics and stabilities of the chiral ion-pairs in the condensed phase with explicitly solvated molecular dynamics (MD) simulations, comparing these results with density functional theory (DFT) calculations. The intermolecular interactions responsible for chiral induction have been identified to elucidate the mode of action and enantioselectivity for the nucleophilic ring opening of aziridinium and episulfonium ions experimentally studied by Toste. We also investigate the deactivation of the catalyst via alkylation. We discuss the suitability of common DFT approaches for the study of these flexible systems and the potential for further developments. The reported results allow us to highlight the factors on which enantioselectivity depends in this and related counteranion-mediated transformations.



Scheme 2. Representative examples of asymmetric counterion-directed catalysis with BINOL phosphates and phosphoramidates. Cat* = chiral catalyst, S = achiral substrate, P* = enantioenriched product.

COMPUTATIONAL DETAILS

MD Simulations. Configurational sampling of ion-pair structures (**Scheme 1**) in different solvents was performed using classical MD simulations. For substrates, OPLS-AA compatible force field parameters were generated using the MacroModel 9.1 force field version 2001 (Schrödinger LLC).³³ Restrained electrostatic potential (RESP) charges were derived by fitting partial charges to HF/6-31G(d) electrostatic potentials calculated using Gaussian 09 (version D.01).³⁴ For episulfonium parameters were taken in analogy to the aziridinium compound, with the only difference being the C-S distances and charges. Four different solvents were considered: toluene, dichloromethane (DCM), acetonitrile (MeCN), and water. The three-point transferable intermolecular potential (TIP3P)³⁵ was used to model water and the optimized potentials for liquid simulations (OPLS) force field for all other solvents. The topologies for toluene, DCM, and MeCN were taken from the GROMACS Molecule & Liquid Database.^{36,37} All the simulations were performed using the GROMACS package (version 5.1.2)^{38,39} using three-dimensional periodic boundary conditions. Long-range electrostatic interactions were treated using the particle mesh Ewald (PME) approach⁴⁰ with a cut-off length of 1.0 nm. A dispersion correction was applied to energy and pressure terms to account for truncation of van der Waals terms.

Initial conformational sampling was used to generate different ion-pair configurations in solution at 298 K. The systems were immersed in a box of solvent with a distance from the border of at least 15 Å. Following steepest descent minimization, the systems were equilibrated in two steps, the first phase involved simulating for 200 ps under a constant volume (NVT) ensemble with position restraints applied to heavy atoms. The temperature was maintained at 298 K using the V-Rescale method. This was followed by 200 ps of constant-pressure (NPT) equilibration using the Parrinello–Rahman pressure coupling⁴¹ algorithm with the compressibility set to 5×10^{-5} bar⁻¹ and the time constant set to 5 ps. A 1 fs time step was used during these stages to allow potential inhomogeneities to

self-adjust. Each system was then equilibrated initially for 100 ns with a 2 fs time step at constant pressure. The first 1 ns was removed from the analysis. The distance between the center-of-mass (COM) of the two ions was used to monitor the interaction of the complexes over time.

The gromos clustering method of GROMACS was employed with the ion-pair complex taken as a reference for centering the system. A root-mean-square deviation (RMSD) criteria of 0.18 nm was used for clustering the conformations. A conformation was classified to a cluster when its distance to any element of the cluster is less than its criteria. From each highly populated cluster, a representative structure that is structurally close to the middle structure of the cluster (based on RMSD criteria) was used as reference for further QM calculations. To investigate the effect of solvent on the preorganization of the ion-pair simulations were also carried out in a box of DCM, MeCN and water.

The potential of mean force (PMF) between the two ions as they separate was calculated using umbrella sampling (US), where ion pairs were held at fixed distances by imposing harmonic restraints. The initial structures for this calculation were generated from a pulling simulation. To initiate these calculations the system was placed in a rectangular box ($5 \times 5 \times 12$ nm³) with dimensions sufficient to satisfy the minimum image convention and provide space for pulling the systems apart along the z-axis. Following steepest descent minimization, the system was equilibrated for 50 ps under a constant volume (NVT) ensemble at 298 K, followed by 50 ps of constant-pressure (NPT) equilibration, using this final structure as starting point for pulling simulations. The phosphate moiety of the catalyst was used as reference for the pulling simulations. The substrate was pulled away from the core structure along the z-axis over 1.6 ns, using a spring constant of 500 kJ mol⁻¹nm⁻² and a pull rate of 0.003 nm ps⁻¹ (3 nm per ns). A final center-of-mass (COM) distance between the catalysts and the substrate of approximately 5.5–6.0 nm was achieved. From these trajectories, snapshots were taken to generate the starting configurations for the US windows. In each window, 100 ps of relaxation with the Berendsen thermostat to reinitialize the system followed by 5 ns of MD was performed, giving a total simulation time of 175 ns per system. Three independent full runs were performed for each system in each solvent. After removing the first 1 ns for equilibration, the PMFs were constructed with the weighted histogram analysis method (WHAM).^{42,43} Statistical uncertainties of the PMFs were estimated using Bayesian bootstrapping of complete histograms.⁴³

DFT Calculations. DFT calculations were performed to investigate the origins of enantioselectivity in the ring-opening step.³⁴ Geometry optimizations were carried out with ω B97X-D⁴⁴ functional and the 6-31G(d) basis set. Vibrational frequencies were computed at the same level of theory to confirm whether the structures correspond to a minimum or a transition state (TS) and to evaluate the zero-point vibrational energy (ZPVE) and thermal corrections at 298 K. Vibrational entropies were corrected ac-

cording to the so-called “quasi-harmonic approach”⁴⁵ using a free-rotor approximation for vibrational modes below 100 cm⁻¹ and a rigid rotor approximation above this cutoff.⁴⁶ Single-point energies were obtained at the ω B97X-D/6-311++G(d,p) level of theory. Optimizations and the subsequent single point energy calculations were carried out in gas phase or in solvent using the SMD solvent model as implemented in Gaussian.⁴⁷ Geometry optimization have also been carried out using the Mo6L(D)⁴⁸ and ω B97X⁴⁴ functionals to analyze the influence of dispersion upon optimized structures and stabilities.

RESULTS AND DISCUSSION

Ion-pair binding modes and interaction energies. To model the association of chiral anion with cationic substrate, we reasoned that explicitly-solvated classical MD

simulation would allow us to generate and sample structures in an unbiased way and to assess stability in response to the surrounding solvent for time-scales inaccessible to QM calculation. Unsurprisingly, synthetic applications of chiral counteranion catalysis generally employ non-polar solvents, such as dichloromethane, chloroform, and toluene. However, other protic and non-protic solvents have also been employed.^{49,50} Since stereocontrol relies on the formation of a strong contact ion-pair, it is instructive to compare the ion-pair stability and lifetime in different environments to provide a better understanding of the factors determining the spectrum of solvents and mixed-solvents suitable for a given transformation. Three different ion-pair complexes were studied, consisting of the cations shown in **Scheme 1** in complex with the (*R*)-TRIP counteranion.

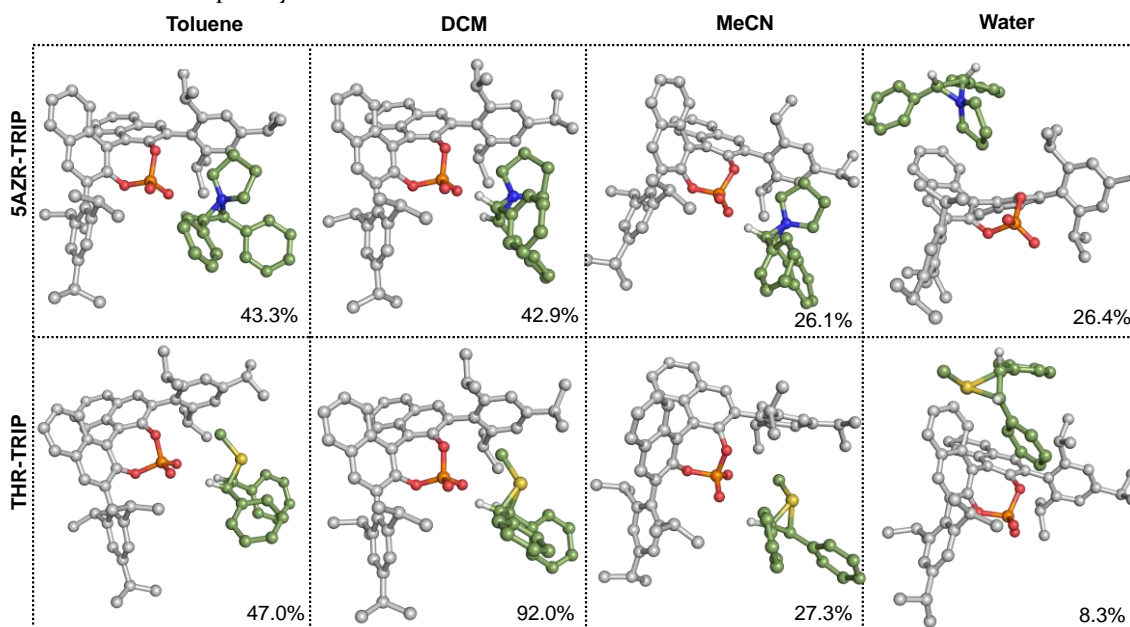


Figure 1. Representative structures of 5AZR-TRIP and THR-TRIP ion-pair complexes at 298K in different solvents, with percentage population. Shown here is the most populated cluster obtained using a RMSD criteria of 1.8 Å. Non-participating hydrogen atoms are omitted for clarity.

Two of them (5AZR and THR) correspond to compounds studied experimentally by Toste,¹⁴ while AZR is a model system used to analyze the influence of bulkiness surrounding the positive charge. Both diastereomers of the *meso*-episulfonium ion were considered: the *trans*-form was found to be more stable and used throughout. Additionally, four different solvents were analyzed including toluene (originally used in ref. ¹⁴), DCM, MeCN and water, which cover a wide range of dielectric constants. In toluene and DCM, the chiral ion-pair complex is stable over 100 ns of unrestrained MD simulation and no dissociation is observed during that time. The situation is markedly different in more polar MeCN and water solvents, where several events of dissociation/association are observed for both aziridinium and episulfonium ion-pairs (**Figure S1-S2**). In MeCN, even though the ion-pair complex is ob-

served, dissociation into separately solvated ions and solvent-shared ion-pairs, in which the substrate and catalyst ions are separated by a single layer of solvent molecules, is also observed.

The formation of stable ion-pairs in toluene and DCM, which exist only transiently in MeCN and water, is consistent with experimental choices of solvent and confirms (as much as possible) the physical realism of the simulations. We thus evaluated the most stable interaction modes by clustering configurations generated over 100 ns (9,900 snapshots when removing the first 1ns), using a RMSD criterion of 1.8 Å (**Figure 1** and **Figures S3-S4**). For the aziridinium-catalyst complex (5AZR-TRIP) at 298 K, 13 and 15 clusters were generated in toluene and DCM, respectively. The first three clusters in each solvent account for 83% and 86% of the total number of conform-

mations sampled, thus demonstrating their stability. In the most stable conformations found for each electrophile the cationic intermediate is positioned inside the catalyst's aromatic pocket, with the two benzylic C-H bonds (α -to N) oriented towards the phosphate O atoms. The ion-pair binding mode for both synthetic substrates are essentially identical in the two most stable conformers. Subsequent QM calculations (discussed later) support the formation of CH \cdots O interactions.⁵¹ When dimethyl aziridinium (AZR-TRIP) is used instead of the five-membered ring (5AZR-TRIP) a slightly different configuration is observed, with the nitrogen atom pointing more closely to the phosphoric acid group and the CH \cdots O interaction less prominent.

In MeCN and water a much larger number of clusters are obtained (393 and 811, respectively). As observed before, in these solvents the ion-pair goes through several events of dissociation-association. In MeCN even though more than 75% of the configurations show the ions being at close distance, many of these configurations are not conducive to ring-opening, that is, the relative position between the ions does not favor the direct interaction between the aziridinium and phosphate groups as found in toluene or DCM (**Figure S3**). This instability is enhanced in aqueous solvent by the competition between water as a strong hydrogen bond donor/acceptor and the chiral catalyst. The three most populated clusters, which account for 37% of all the configurations, show the ions being close to each other but separated by solvent molecules (**Figure 1** and **S3**). In such case, an average of five water molecules are found inside the catalyst pocket, with at least two of them solvating each free oxygen of the catalyst (**Figure S5**). Rueping and Thiesmann have previously demonstrated Brønsted acid-catalyzed hydrogenation of quinolines in aqueous media as a consequence of hydrophobic hydration.⁵⁰ A similar effect seems unlikely in this case, as electrostatic interactions largely dominate the reorganization of the solvent around the ions. For neutral, and in particular, relatively large hydrophobic solutes, hydrophobic hydration may dominate if polar solvent molecules can reorganize near them without sacrificing hydrogen bonds.⁵²

For the episulfonium-catalyst (THR-TRIP) at 298K a smaller number of clusters are observed in toluene and DCM compared to 5AZR-TRIP (9 and 7, respectively). The first three clusters in each solvent account for 95% and 99% of the total number of conformations sampled in each solvent (**Figure 1** and **S4**). As observed before, the stability of this arrangement decreases in polar solvents, leading to 602 and 986 clusters in MeCN and water, respectively. While in MeCN the ion-pair complex is still observed in some configurations, in water the solvent separated ion-pair dominates.

Potentials of Mean Force. To evaluate the ion-pair interaction energies, the potential of mean force (PMF) for the ion-pair dissociation was calculated at 298K in explicit solvent (**Figure 2** and **S6** and **Table 1**). Examination of these data confirms that the interaction diminishes as the

solvent becomes more polar. As expected from the dominant Coulombic term, the interaction energy depends linearly with the inverse of the solvent dielectric constant (**Figure S7**). Taking 5AZR-TRIP as an example, the ion-pair dissociation energy (ΔG) decreases from 44 kcal \cdot mol $^{-1}$ in toluene ($\epsilon = 2.38$) kcal \cdot mol $^{-1}$ to 14 kcal \cdot mol $^{-1}$ in DCM ($\epsilon = 8.9$) and then to 3 kcal \cdot mol $^{-1}$ in water ($\epsilon = 80.1$). In toluene, at distances between 6 and 10 Å (measured between the centers of mass of the respective ions), a contact ion pair is still observed, with both ions sharing a common solvation shell (**Figure 2B**). As the ions start to separate a shared solvation shell forms between them (around 13 Å). Only at distances larger than 20 Å do the ions become independently solvated. This long-range effect is particularly strong in toluene. For solvents with higher dielectric constant, such as in DCM the ion-pair interaction is weaker and long-range effects are reduced. In MeCN ($\epsilon = 37.5$) the interaction between the ions (even though in an unproductive conformation) is more dominant than in water, where the independently solvated species are the most stable ones. In both cases the energy associated with their electrostatic attraction is just slightly larger than the thermal energy at room temperature available to separate them ($kT \cdot N_A = 0.59$ kcal \cdot mol $^{-1}$). This suggests that even though ion-pairing is possible, any stability in polar solvent is short-lived and highly-dependent on concentration/temperature effects.

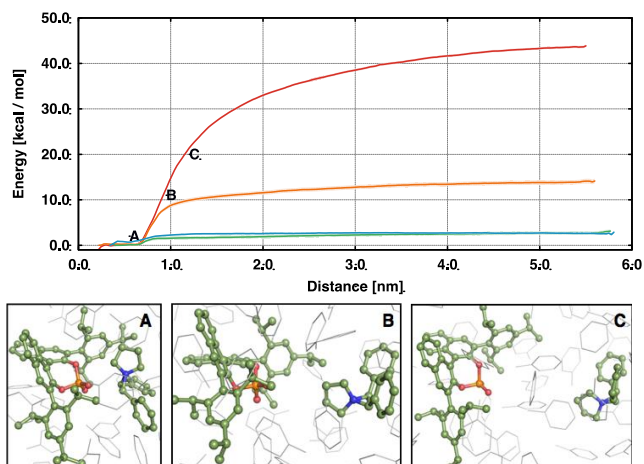


Figure 2. (top) Potential of mean force (PMF) profiles for the complex dissociation of the 5AZR-TRIP ion-pair in toluene (red), dichloromethane (DCM, orange), acetonitrile (MeCN, green) and water (blue). (bottom) Representative configuration states (A–C) along the PMF in toluene.

QM Interaction Energy. To further analyze the ion-pair complexes we carried out DFT calculations using Mo6-L(D) and the ω B97X(D) functionals with and without atom-pairwise dispersion corrections. Geometry optimizations were initiated from the most stable structures in **Figure 1**, separately in gas phase and with SMD implicit solvent corresponding to toluene. DFT optimized structures are shown in **Figure S8** and interaction energies tabulated in **Table S1**. Despite the low polarity of toluene, the inclusion of implicit solvent has a notable effect upon

the ion-pair geometry (see **Tables S2** and **S3**): the counterion separation, measured between the P and N or S atoms, lengthened by up to 0.17 Å (on average 0.08 Å) relative to gas-phase structures with CH-O distances similarly lengthened by up to 0.11 Å (average of 0.06 Å). The inclusion of dispersion was also found to affect both structures and energetics: the explicit dispersion term in ω B97X-D (which used uses a modified version of Grimme's D2 dispersion correction⁵³) lead to tighter and more stable complexes by up to 8 kcal·mol⁻¹ (**Table S1**). Except for water, the differential ion-pair stabilities as a function of solvent was very well described. Mo6-L is a local meta-GGA functional, which performs best in its description of non-covalent interactions among the local (i.e. non-hybrid) Minnesota functionals,⁵⁴ and the absence of exact exchange leads to reduced computational cost. The explicit inclusion of dispersion was found to improve the Mo6-L results (Mo6L-D3), giving more favorable interaction energies which agree more closely with those obtained in explicit solvent. Nevertheless, SMD- ω B97X-D association free energies most closely reproduce those obtained from the PMF in explicit solvent across the range of solvents studied and so this methodology was pursued in subsequent studies.

Ion-pair complex formation is enthalpically driven, in line with the electrostatic nature of the interaction energies expressed at the first order by a Coulomb potential. How-

ever, there is an entropic penalty due to the loss of translational and rotational entropy upon binding. Interaction free energies from MD and QM show a good qualitative correlation, although QM values are systematically smaller (i.e. less favorable) than the ones obtained from MD. As seen in **Table S4** an almost constant entropic cost ($-T\Delta S = 16$ -17 kcal·mol⁻¹) is obtained from QM data, irrespective of whether calculations are performed in gas or solution phase. This term is dominated by the loss of rotational and translational degrees of freedom, for which the ideal gas approximation is expected to overestimate the unfavorability since the confining effect of surrounding solvent molecules is not considered. We attribute the weaker association free energies obtained from DFT vs. MD results to this overestimated entropic term.

Scheme 3. Model catalysts studied in this work.

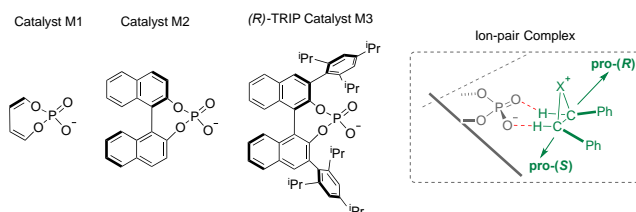


Table 1. Interaction energies (kcal·mol⁻¹) calculated using MD simulations (PMF over three independent runs in the respective solvents at 298.15K) and using QM calculations at the (SMD)- ω B97X-D/6-311++G(d,p)/(SMD)- ω B97X-D/6-31G(d) level of theory. *25°C

Solvent	ϵ_{20C}	AZR-TRIP		5AZR-TRIP		THR-TRIP	
		ΔG_{MD}	ΔG_{QM}	ΔG_{MD}	ΔG_{QM}	ΔG_{MD}	ΔG_{QM}
Gas	1.00	--	-75.7	--	-77.5	--	-82.2
Toluene	2.38	-43.4±0.3	-33.0	-43.6±0.1	-34.8	-47.4±0.2	-39.0
DCM	8.93*	-14.3±0.2	-7.8	-14.0±0.1	-10.0	-17.2±0.1	-11.2
MeCN	37.50	-2.6±0.2	-0.3	-2.8±0.2	-3.4	-2.9±0.1	-2.6
Water	80.10	-0.5±0.2	-1.8	-2.6±0.1	-3.5	-1.5±0.1	-1.6

Both 5AZR-TRIP and THR-TRIP ion-pair complexes behave similarly in terms of geometries and interaction energy. The slightly larger interaction energy for the episulfonium complex is related to the slightly closer interaction between the two ions evidenced by the shorter CH...O distances (**Table S5**). Once in contact with a chiral counteranion the electrophile's benzylic carbon atoms are distinguishable, so we considered whether one site is clearly activated in the ion-pair. We refer to these positions as pro-(*R*) and pro-(*S*), where attack at each of them leads to the (*R,R*) or (*S,S*) product, respectively (**Scheme 3**). In the ground state ion-pair struc-

ture the pro-(*S*) carbon (which leads to the major enantiomer, has a slightly more positive charge than pro-(*R*).

The absence of strongly directional interactions in contact ion-pairs means that chemical intuition alone may be insufficient to survey the accessible binding modes.⁵⁵ From our MD-based sampling of three ion-pairs we find a single binding mode (shown in **Figure 1**) present in the most populated complex for each system in apolar solvent. Based on this ion-pair geometry we studied the nucleophilic ring-opening with DFT calculations. We studied three different models of the phosphate counterion (**Scheme 3**), which help to establish

the origins of stereinduction. Model 1 (M1) lacks the chiral BINOL backbone, while in Model 2 (M2) the isopropyl groups have been removed and Model 3 (M3) corresponds to the full TRIP counterion used by Toste in ref. 14. For both aziridinium and episulfonium ions a more stable complex is formed when catalyst M3 is used. No clear correlation is seen between computed charges on the anion catalyst and the cationic $C_2H_2X^+$ moiety (Table 2), indicating that not only electrostatic, but also van der Waals interactions between substrate and triisopropylphenyl groups stabilize the complex with catalyst M3. The existence of favorable nonbonding interactions between the substrate and one of the catalyst's aromatic groups can be seen by computing the non-covalent interaction⁵⁶ (NCI) index from the electron density of each system (Figure 3). The NCI analysis also confirms the presence of attractive $CH\cdots O$ interactions between substrate CH groups and phosphate oxygens. These $CH\cdots O$ interactions have been shown to play a crucial role in many asymmetric reactions.^{57–61} $CH\cdots O$ interactions are generally weaker than classical hydrogen bonds⁵¹; however, the presence of a positive charge on the proton donor as well as sp^2 -like hybridization on the carbon center, as is the case here, are expected to magnify their HB strength.⁶²

Ring-Opening. We obtained the DFT-computed free energy profile for the ring opening of *meso*-aziridinium (5AZR) and *meso*-episulfonium (THR) by neopentyl alcohol in toluene. Initially, the ion-pair complex and alcohol nucleophile form a reactant state (RS) complex involving a hydrogen bond between the OH group of the nucleophile and one of the phosphate O atoms. Compared with the separated species (ion-pair + nucleophile), the RS is lower in energy (ΔG) by 2–3 kcal·mol^{−1} when the M2 and M3 catalyst are used. However, it is unfavorable with the smaller M1 catalyst. This is observed for both 5AZR and THR (Figure 4). Irreversible nucleophilic addition proceeds through a single stereodeter-

mining S_N2 transition structure (TS), in which attack occurs at either benzylic carbon $C_{pro-(R)}/C_{pro-(S)}$ leading to (*R,R*) or (*S,S*) product, respectively. As with experiment, the (*R*)-catalyst leads preferentially to the (*S,S*) product. Experimentally, for catalyst M1 no selectivity would be obtained, since this is achiral (due to rapid rotation around the diene backbone). However, we preserved the catalyst conformation and interaction modes of the larger (axially chiral) systems, to probe the effects of the flanking aromatic groups in these catalysts. With the M3 catalyst the activation energy is 15.4 and 1.2 kcal·mol^{−1} for the ring-opening of 5AZR and THR in toluene, respectively. This is substantially lower than the activation energy in the uncatalyzed reaction, which is found to be 32.1 and 16.0 kcal·mol^{−1} for 5AZR and THR, respectively (Table 3 and Figure 5).

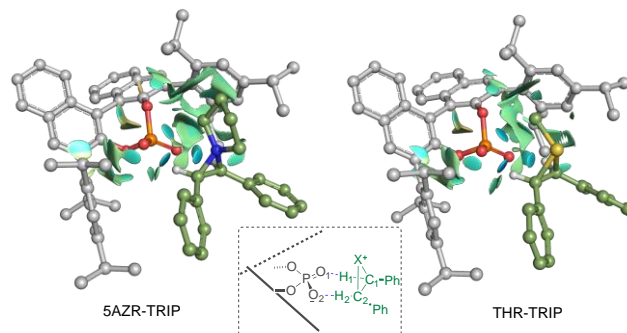


Figure 3. Non-covalent interaction (NCI) isosurface (0.05 a.u.) for the ion-pair complex. An identifiable $CH\cdots O$ interaction (cyan circles) between the CH groups of the substrate and the catalyst's oxygen is observed.

Table 2. SMD- ω B97X-D/6-311++G(d,p)//SMD- ω B97X-D/6-31G(d) CHelpG charges for the atoms forming the 3-membered ring ($C_2H_2X^+$), phosphate group (PO_4^-) and PA catalyst as a whole (Cat). Interaction free energies (in kcal·mol^{−1}) at the same level of theory in toluene are also presented.

5AZR-TRIP		ESP Charges				Distances		
Model	Energy	$C_{pro-(R)}$	$C_{pro-(S)}$	$C_2H_2N^+$	PO_4^-	Cat	$CH_{pro-(R)}-O_1$	$CH_{pro-(S)}-O_2$
M1	−26.7	−0.02	0.03	0.30	−1.06	−0.65	2.00	2.02
M2	−26.9	0.02	0.05	0.27	−1.26	−0.88	2.15	2.16
M3	−34.8	0.03	0.06	0.31	−1.08	−0.83	2.10	2.03
THR-TRIP		ESP Charges				Distances		
Model	Energy	$C_{pro-(R)}$	$C_{pro-(S)}$	$C_2H_2S^+$	PO_4^-	Cat	$CH_{pro-(R)}-O_1$	$CH_{pro-(S)}-O_2$
M1	−31.3	−0.02	0.20	0.38	−1.01	−0.81	1.92	2.04
M2	−32.2	−0.08	0.09	0.36	−1.23	−0.87	2.04	2.18
M3	−39.0	−0.01	0.26	0.36	−1.05	−0.80	2.10	1.96

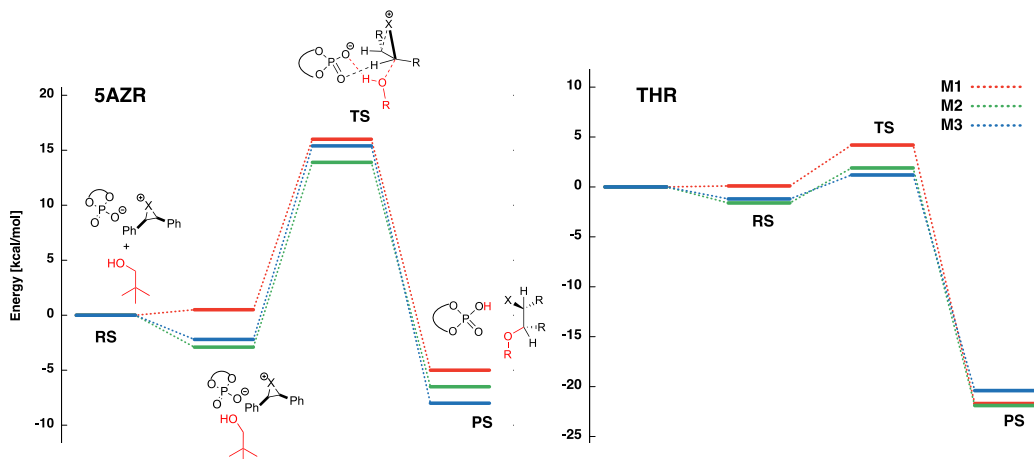


Figure 4. The catalyzed ring-opening of *meso*-aziridinium (5AZR) and *meso*-episulfonium (THR) in toluene. Only the preferred (*S,S*) pathway is shown here. Energies in kcal·mol⁻¹.

Solvent is found to increase the activation barrier for both the uncatalyzed and catalyzed process compared to gas phase (Table S6). However, the catalytic effect is similar in both cases. In the absence of catalyst, the nucleophilic ring-opening step is highly endergonic (by at least 13.0 kcal·mol⁻¹) – proton transfer to the counteranion ensures that this step is favorable.

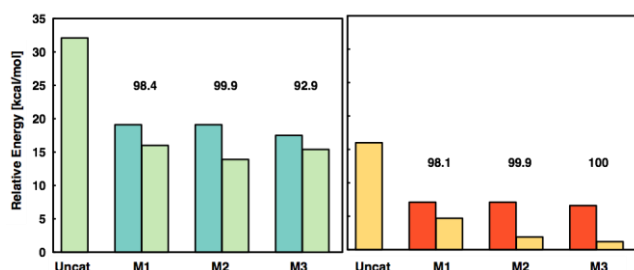


Figure 5. Activation free energy for the uncatalyzed (uncat) and catalyzed 5AZR (green) and THR (orange) ring opening process in gas phase and toluene. TS(*R,R*) in dark grey/orange and TS(*S,S*) in light green/orange. Free energies in kcal·mol⁻¹.

The TS for each of these pathways are shown in Figure 6. In accordance with the Hammett postulate, as the energy barrier drops an earlier (looser) transition state is observed. Compared to the uncatalyzed process, the O_{nuc}-C bond increases from 1.9 (2.0) Å to 2.0 (2.3) Å for 5AZR (THR), while the C-X⁺ distance remains relatively constant for 5AZR and is slightly tighter for THR (Table S7). This is also more prominent in the lowest-energy TS (*S,S*). In all cases, the alcohol proton was transferred to the catalyst oxygen during this step. This occurs asynchronously, after ring-opening as the TS relaxes to the product. In the lower energy TS (*S,S*) a CH...O interaction between substrate and catalyst occurs, involving the carbon which is attacked. The influence of this interaction upon selectivity is discussed below.

From these TSs it can also be seen that the nucleophile's alkyl chain is oriented away from the catalyst and so a wide range nucleophiles will be tolerated. This is in line with the experimental results by Toste, which demonstrate that a wide spectrum of nucleophiles could be used in this transformation without loss of selectivity. Despite the differences in complex stability for both the ion-pair and the reactant complex, the three models favor the same absolute (*S,S*) sense of enantioselectivity in the ring-opening TSs with a similar magnitude, thus suggesting that the key interactions driving enantioselectivity are present in the minimal model, for which steric interactions are largely absent.

Table 3. Reaction free energy (in kcal·mol⁻¹) at the SMD-ωB97X-D/6-311++G(d,p)//SMD-ωB97X-D/6-31G(d) level of theory.

Model	5AZR-TRIP			THR-TRIP		
	ΔG [‡]	ΔG _{rxn}	%ee	ΔG [‡]	ΔG _{rxn}	%ee
Expt.	--	--	94	--	--	91
M1	TS(<i>R,R</i>)	19.1	-1.2	7.1	-9.8	98.1
	TS(<i>S,S</i>)	16.0	-5.0	4.7	-21.1	
M2	TS(<i>R,R</i>)	19.1	1.6	7.1	-11.5	99.9
	TS(<i>S,S</i>)	13.9	-6.5	1.9	-21.9	
M3	TS(<i>R,R</i>)	17.5	-1.9	6.6	-13.8	100.0
	TS(<i>S,S</i>)	15.4	-8.0	1.2	-20.4	
Uncat		32.1	26.7		16.0	13.0

Energies relative to the separated ion-pair complex and nucleophile; for the uncatalyzed systems energies relative to the separated nucleophile and substrate.

While the most stable ion-pair complex was obtained with the more sterically demanding (M3) catalyst, the higher enantioselectivity is obtained with the chiral but less bulky (M2) catalyst. M2 also led to a slightly more stable RS complex compared to M3, probably due to the

stronger interaction between the nucleophile and the oxygen of the catalyst. This result shows that even though formation and stability of the ion-pair complex is essential and favored by more sterically demanding catalysts, quantitative correlation between interaction energy and catalysis/selectivity is less straightforward. In each case, comparing against experimental selectivities the absolute sense of enantioselectivity is correctly computed. Taking as an example the 5AZR-TRIP and THR-TRIP using the full catalyst (for which experimental data are available) %ee values of 92.9 and 100 are obtained, respectively, which compare well with the experimental values of 94% and 91%, respectively.¹⁴ Better quantitative agreement is obtained for the aziridinium desymmetrization, with an error in terms of $\Delta\Delta G^\ddagger$ of 0.12 kcal·mol⁻¹ whereas in the episulfonium case selectivity is overestimated by 3.4 kcal·mol⁻¹. Alternative coordination modes involving the minor episulfonium diastereomer (with Me *cis*- to the Ph-rings) may be a contributing factor here.

To trace back the origin of enantioselectivity we performed distortion/interaction analysis⁶³. In this analysis, the activation energy of a process (ΔE^\ddagger) is partitioned into

the energy required to distort the reactants from their ground-state geometry to their transition state geometry ($\Delta E_{\text{dist}}^\ddagger$) and the energy of interaction between these distorted fragments ($\Delta E_{\text{int}}^\ddagger$). For the system under study, these quantities were obtained by separating each transition state structure into three fragments (catalyst, substrate and nucleophile) and calculating the energy differences ($\Delta E_{\text{dist_cat}}^\ddagger$, $\Delta E_{\text{dist_sub}}^\ddagger$ and $\Delta E_{\text{dist_nuc}}^\ddagger$) between the distorted and ground-state structures. The interaction energy ($\Delta E_{\text{int}}^\ddagger$) is then obtained as the difference between the activation energy (ΔE^\ddagger) and the total distortion energy ($\Delta E_{\text{dist}}^\ddagger = \Delta E_{\text{dist_cat}}^\ddagger + \Delta E_{\text{dist_sub}}^\ddagger + \Delta E_{\text{dist_nuc}}^\ddagger$).

The energy components for each transition-state model (M1-M3) and the values are tabulated in **Table 4**. The differential components are shown for aziridinium opening in **Figure 7**, from which it can be seen that for smaller models M1 and M2, the difference in interaction energies is decisive, while the difference in distortion energies is small: the major TS(S,S) benefits from a more favorable interaction energy.

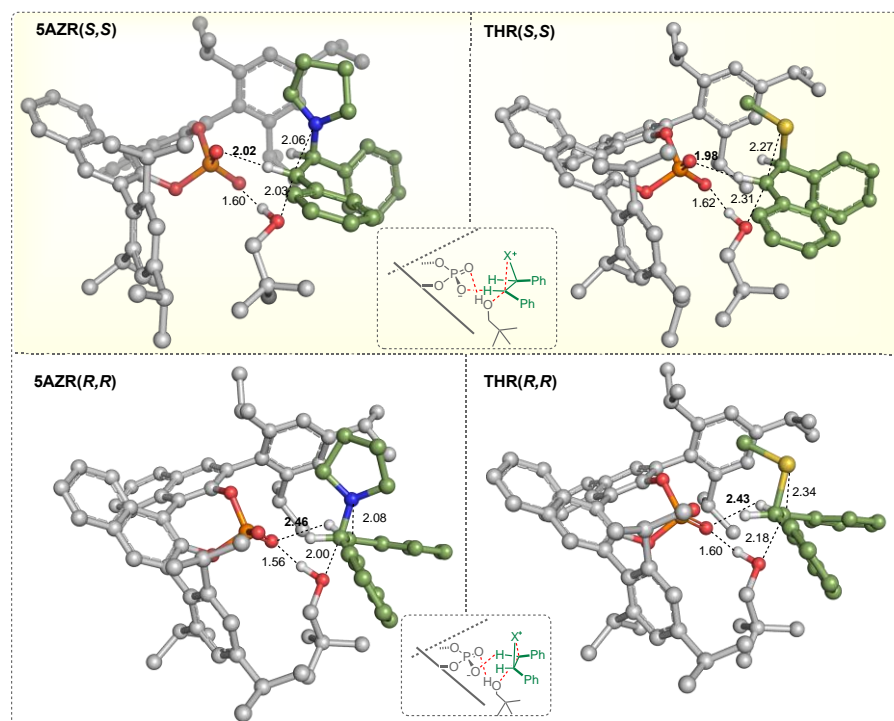


Figure 6. TSs for the catalyzed ring-opening of *meso*-aziridinium (5AZR) and *meso*-episulfonium (THR) in toluene. Relevant distances shown in Å

Table 4. Distortion/Interaction Analysis for the nucleophilic attack on 5AZR and THR with different catalysts (M1-M3). Shown here are the distortion energies of the catalyst ($\Delta E_{\text{dist_cat}}^\ddagger$), substrate ($\Delta E_{\text{dist_sub}}^\ddagger$) and nucleophile ($\Delta E_{\text{dist_nuc}}^\ddagger$), the interaction energies ($\Delta E_{\text{int}}^\ddagger$) and the activation energies (ΔE^\ddagger). All energies are given in kcal·mol⁻¹.

M1			M2			M3		
TS(R,R)	TS(S,S)	$\Delta\Delta E$	TS(R,R)	TS(S,S)	$\Delta\Delta E$	TS(R,R)	TS(S,S)	$\Delta\Delta E$

5AZR-TRIP									
$\Delta E_{\text{dist_cat}}^{\ddagger}$	0.4	0.4	0.0	0.6	0.4	-0.2	0.2	1.1	0.9
$\Delta E_{\text{dist_sub}}^{\ddagger}$	22.9	21.5	-1.4	23.4	22.0	-1.4	26.3	21.7	-4.6
$\Delta E_{\text{dist_nuc}}^{\ddagger}$	0.6	1.9	1.3	0.6	1.6	1.0	1.3	1.1	-0.2
$\Delta E_{\text{dist}}^{\ddagger}$	23.9	23.8	-0.1	24.6	24.0	-0.6	27.8	23.9	-3.9
$\Delta E_{\text{int}}^{\ddagger}$	-5.2	-7.0	-1.8	-2.8	-6.6	-3.8	-7.5	-5.3	2.2
ΔE^{\ddagger}	18.7	16.8	-1.9	21.8	17.4	-4.4	20.3	18.6	-1.7
THR-TRIP									
$\Delta E_{\text{dist_cat}}^{\ddagger}$	1.9	0.0	-1.9	0.5	0.1	-0.4	-0.2	1.0	1.2
$\Delta E_{\text{dist_sub}}^{\ddagger}$	7.0	5.5	-1.5	7.9	5.5	-2.4	10.9	5.0	-5.9
$\Delta E_{\text{dist_nuc}}^{\ddagger}$	-0.1	1.0	1.1	-0.2	0.7	0.9	0.6	0.4	-0.2
$\Delta E_{\text{dist}}^{\ddagger}$	8.8	6.5	-2.3	8.2	6.3	-1.9	11.3	6.4	-4.9
$\Delta E_{\text{int}}^{\ddagger}$	-2.4	-2.8	-0.4	-0.2	-3.3	-3.1	-3.2	-2.3	0.9
ΔE^{\ddagger}	6.4	3.7	-2.7	8.0	3.0	-5.0	8.1	4.1	-4.0

This is consistent with a greater CH \cdots O interaction in the (S,S) TS, supported by $n_X-\sigma^*_{C-H}$ delocalization energies calculated through second order perturbation theory⁶⁵ (Table S8). The calculated $O_{lp}-\sigma^*(C-H)$ $E(2)$ stabilization energy is larger for the TS(S,S) pathway compared to the TS(R,R) one.

In contrast, for the larger model M₃, it is the difference in distortion energies which is the larger term and controls the selectivity. This is due to substrate distortion, which rises noticeably in TS(R,R) for model M₃ by more than 3 kcal·mol⁻¹ compared to the other models, whereas for TS(S,S) there is no such increase. There are no close steric contacts (i.e. intermolecular H-H distances less than the sum of the Van der Waals radii) between the catalyst and either the nucleophile or the substrate in any of the TS models.

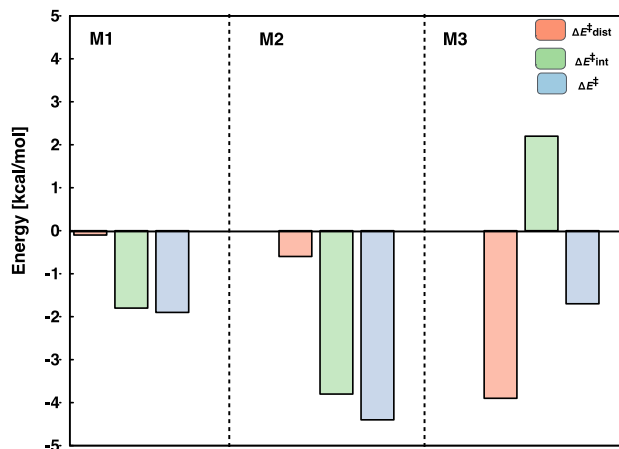


Figure 7. Relative distortion (red), interaction (green) and total (blue) energy values ($\Delta\Delta E_{SS-RR}$) for each catalyst model. Negative values favor TS(S,S) while positive value favor TS(R,R). Energies in kcal/mol.

Nor are repulsive regions visible in NCI-plots (see Figure S10). However, the alleviation of steric interactions with the catalyst do play a decisive role since they incur the cost of greater substrate distortion in TS(R,R). Indeed, superimposition of the TSs across different models shows very little change in substrate binding mode for the major (S,S) structures, whereas noticeable twisting of the substrate occurs in the minor (R,R) TS once the bulkier M₃ catalyst substituents are introduced (see Figure S11 for overlay). This is necessary to avoid clashes between one of the substrate's phenyl rings and a catalyst isopropyl group. This also results in rotation of the phenyl rings, and it is this rotation which is responsible for the larger substrate distortion energy which disfavors this TS. We note that previously, unfavorable steric interactions were found to result in catalyst, rather than substrate, distortion.⁶⁴

Catalyst deactivation. Degradation of the catalyst by means of direct nucleophilic attack of the phosphate may be expected when using highly reactive electrophiles. This pathway has been reported, for example, with epoxides⁶⁶⁻⁶⁸ and aziridines^{69,70}, the later being extremely useful for DNA alkylation. As a way to suppress catalyst degradation, the concept of using a carboxylic acid as co-catalyst has been developed by List and coworkers.^{68,71} Reaction kinetic analysis showed that, in the absence of carboxylic acid and increasing catalyst concentration, direct alkylation of the catalyst by the electrophile (such as epoxide or aziridine) dominates. Carboxylic acid additives in phosphoric acid-catalysis were also reported by Rueping⁷² and Antilla.⁷³

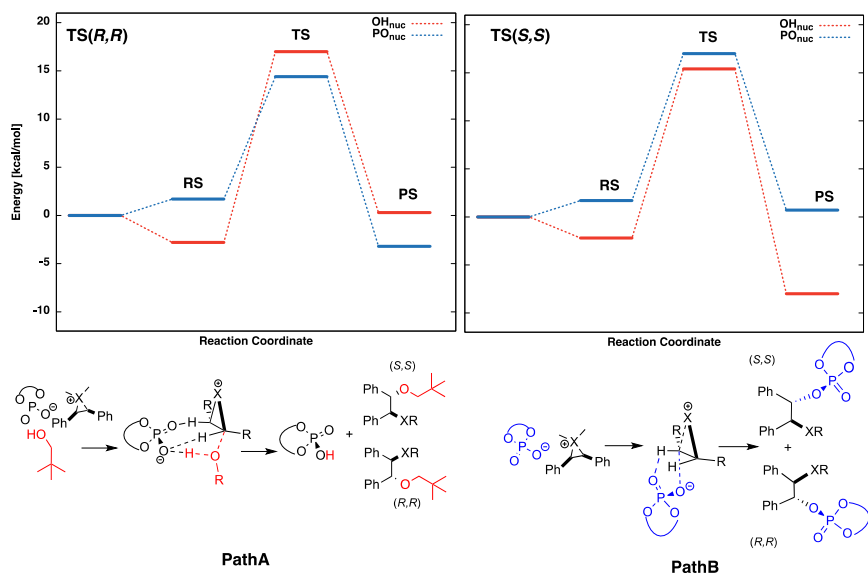


Figure 8. Competing reactions pathway. Path A corresponds to the nucleophilic attack by alcohol and Path B to the deactivation of the catalyst via alkylation.

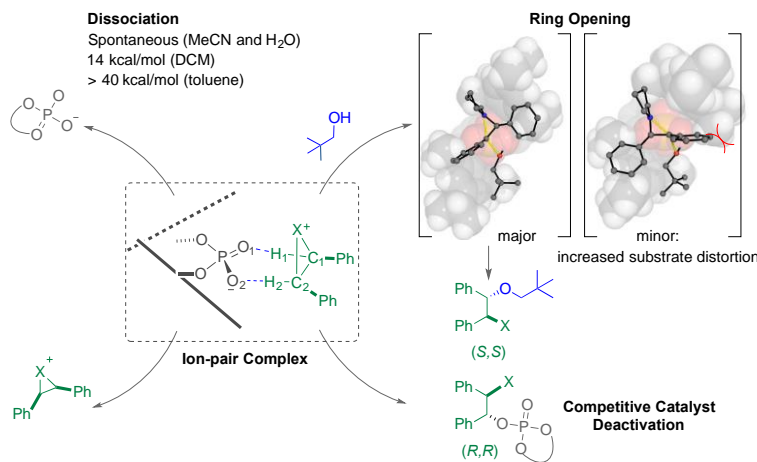
We evaluated this process by modeling the alkylation of the catalyst by the aziridinium (5AZR) substrate. The energetics for this pathway are presented in **Figure 8** and **Table 5** and compared with the ring-opening reaction by alcohol. As can be seen, energies are comparable to the ring-opening by alcohol. Consequently, under stoichiometric conditions, both reactions will compete and the decomposition pathway, even for the sterically hindered catalyst, can occur. Under the reactions conditions used by Toste and coworkers, which include the use of four equivalents of the alcohol nucleophile, no alkylation of the catalyst was reported. This suggests an excess of the nucleophile is necessary to overcome the 1 kcal·mol⁻¹ preference for the deactivation pathway (14.4 vs. 15.4 with M3) and prevent this otherwise viable pathway.

Table 5. Reaction free energy for the nucleophilic attack of the catalyst on the substrate at the SMD- ω B97X-D/6-311++G(d,p)//SMD- ω B97X-D/6-31G(d) level of theory.^a

Nucleophile		Alcohol (Path A) ^b		PA (Path B) ^b	
Model		ΔG^\ddagger	ΔG_{rxn}	ΔG^\ddagger	ΔG_{rxn}
M1	TS(R,R)	19.1	-1.2	14.4	-5.7
	TS(S,S)	16.0	-5.0	13.1	-6.1
M2	TS(R,R)	19.1	1.6	15.4	-13.3
	TS(S,S)	13.9	-6.5	14.3	-5.9
M3	TS(R,R)	17.5	-1.9	14.4	-3.2
	TS(S,S)	15.4	-8.3	17.0	0.7

^aFree energies relative to the separated ion-pair complex and nucleophile. ^bRelative to the ion-pair complex system. All energies in kcal·mol⁻¹

Scheme 4. Summary of the processes studied in this work including: formation/dissociation of the ion-pair species, nucleophilic attack of the 3-membered ring, and catalyst deactivation.



CONCLUSIONS

Chiral phosphate anions have emerged as a powerful way to promote a wide range of asymmetric transformations of positively charged intermediates. However, a theoretical understanding of how these catalysts impart enantioselectivity, for substrates incapable of forming hydrogen bonds has been lacking to date.

In this work, we have presented the first theoretical study into a defining example of chiral anion phase transfer catalysis: the ring-opening of *meso*-aziridinium and episulfonium cations by asymmetric counteranion-directed catalysis (ACDC). Through extensive sampling of the ion-pair system in different environment and a detailed mechanistic study of ion-pairing, ring-opening and catalyst deactivation we were able to explain the experimentally observed enantioselectivity.

Our analysis show that formation/dissociation of the ion-pair, as well as the dominant binding modes, strongly depends on the solvent environment, which is critical for the reaction to take place. Bulkier catalysts favor the stability of the ion-pair as well as formation of a stable complex with nucleophile. Once the ion pair complex is formed, selectivity is primarily determined by the distortion energy of the substrate, which becomes less demanding for the TS(*S,S*) pathway. In this arrangement, the substrate aligns to position the C-H bonds α -to nitrogen or sulfur in the same plane as the P=O group, leading to favorable CH \cdots O interactions between substrate and catalyst. This stabilization occurs at short range, while the attractive electrostatic interaction between the two ions operates over a longer length-scale. Both effects are essential for enantioselectivity. Steric effects contribute to the stability of the ion-pair complex, however, play only a minor role in controlling selectivity in the competing TSs. Instead, the major enantiomer results from a minimization of substrate distortion. This work, summarized by **Scheme 4**, illustrates how different insights into counterion-catalysis are accessible through complementary classical simulations and quantum calculations and provides a rationale for observed selectivities for a range of reactions.

ASSOCIATED CONTENT

Supporting Information

The Supporting Information is available free of charge on the ACS Publications website at DOI: xxx

Analysis of MD simulations and representative clusters; NBO delocalization energies; energetics for the different reaction pathways; absolute energies (a.u.) and selected distances for all DFT computed structures (PDF). Archive of Cartesian coordinates (in xyz format) for computed stationary points (ZIP). Archive of MD containing topologies and input files (ZIP).

AUTHOR INFORMATION

Corresponding Authors

*fernanda.duarte@ed.ac.uk; robert.paton@chem.ox.ac.uk

ACKNOWLEDGMENT

This research was supported financially by the Royal Society (RG110617 to RSP and a Newton Fellowship to F.D.). The authors would like to acknowledge the use of the University of Oxford Advanced Research Computing (ARC) facility in carrying out this work. <http://dx.doi.org/10.5281/zenodo.22558>. We thank an anonymous referee for helpful suggestions in interpreting the distortion-interaction analysis.

ABBREVIATIONS

ACDC: asymmetric counteranion-directed catalysis; CPA: chiral phosphoric acids; DCM: dichloromethane DFT: density functional theory; HB: hydrogen-bonding; INT: intermediate; IRC: intrinsic reaction coordinate; MD: molecular dynamics; MeCN: acetonitrile; OPLS: optimized potentials for liquid simulations; PS: product state; PTC: phase-transfer catalysis; RS: reactant state; SMD: solvent model density and TIP3P: three-point transferable intermolecular potential; TS: transition state

REFERENCES

- (1) Shapiro, N. D.; Rauniyar, V.; Hamilton, G. L.; Wu, J.; Toste, F. D. *Nature* **2011**, 470, 245.

- (2) Phipps, R. J.; Hamilton, G. L.; Toste, F. D. *Nat. Chem.* **2012**, *4*, 603.
- (3) Brak, K.; Jacobsen, E. N. *Angew. Chem. Int. Ed.* **2013**, *52*, 534.
- (4) Mahlau, M.; List, B. *Angew. Chem. Int. Ed.* **2013**, *52*, 518.
- (5) Mayer, S.; List, B. *Angew. Chem. Int. Ed.* **2006**, *45*, 4193.
- (6) Rueping, M.; Uria, U.; Lin, M.-Y.; Atodiresei, I. *J. Am. Chem. Soc.* **2011**, *133*, 3732.
- (7) Terada, M.; Tanaka, H.; Sorimachi, K. *J. Am. Chem. Soc.* **2009**, *131*, 3430.
- (8) Shi, S.-H.; Huang, F.-P.; Zhu, P.; Dong, Z.-W.; Hui, X.-P. *Org. Lett.* **2012**, *14*, 2010.
- (9) Parmar, D.; Sugiono, E.; Raja, S.; Rueping, M. *Chem. Rev.* **2014**, *114*, 9047.
- (10) Fleischmann, M.; Drettwan, D.; Sugiono, E.; Rueping, M.; Gschwind, R. M. *Angew. Chem. Int. Ed.* **2011**, *50*, 6364.
- (11) Kim, H.; Sugiono, E.; Nagata, Y.; Wagner, M.; Bonn, M.; Rueping, M.; Hunger, J. *ACS Catal.* **2015**, *5*, 6630.
- (12) Greindl, J.; Hioe, J.; Sorgenfrei, N.; Morana, F.; Gschwind, R. M. *J. Am. Chem. Soc.* **2016**, *138*, 15965.
- (13) Sorgenfrei, N.; Hioe, J.; Greindl, J.; Rothermel, K.; Morana, F.; Lokesh, N.; Gschwind, R. M. *J. Am. Chem. Soc.* **2016**, 16345.
- (14) Hamilton, G. L.; Kanai, T.; Toste, F. D. *J. Am. Chem. Soc.* **2008**, *130*, 14984.
- (15) In Toste's experimental work (ref. 14) the absolute configuration of the -TRIP counteranion used is (S) and the major enantiomer formed is the (R,R)-adduct. In the text we refer to the ent-reaction.
- (16) Simón, L.; Goodman, J. M. *J. Am. Chem. Soc.* **2008**, *130*, 8741.
- (17) Simón, L.; Goodman, J. M. *J. Am. Chem. Soc.* **2009**, *131*, 4070.
- (18) Marcelli, T.; Hammar, P.; Himo, F. *Chem. Eur. J.* **2008**, *14*, 8562.
- (19) Marcelli, T.; Hammar, P.; Himo, F. *Adv. Synth. Catal.* **2009**, *351*, 525.
- (20) Yamanaka, M.; Itoh, J.; Fuchibe, K.; Akiyama, T. *J. Am. Chem. Soc.* **2007**, *129*, 6756.
- (21) Yamanaka, M.; Hirata, T. *J. Org. Chem.* **2009**, *74*, 3266.
- (22) Reid, J. P.; Simón, L.; Goodman, J. M. *Acc. Chem. Res.* **2016**, *49*, 1029.
- (23) Jindal, G.; Sunoj, R. B. *Angew. Chem. Int. Ed.* **2014**, *53*, 4432.
- (24) Simón, L.; Paton, R. S. *Org. Biomol. Chem.* **2016**, *14*, 3031.
- (25) Xie, Y.; Cheng, G.-J.; Lee, S.; Kaib, P. S. J.; Thiel, W.; List, B. *J. Am. Chem. Soc.* **2016**, *138*, 14538.
- (26) Raskatov, J. A.; Thompson, A. L.; Cowley, A. R.; Claridge, T. D. W.; Brown, J. M. *Chem. Sci.* **2013**, *4*, 3140.
- (27) Knowles, R. R.; Jacobsen, E. N. *Proc. Nat. Acad. Sci.* **2010**, *107*, 20678.
- (28) Peng, Q.; Duarte, F.; Paton, R. S. *Chem. Soc. Rev.* **2016**, *45*, 6093.
- (29) Lam, Y.-h.; Grayson, M. N.; Holland, M. C.; Simon, A.; Houk, K. N. *Acc. Chem. Res.* **2016**, *49*, 750.
- (30) Wheeler, S. E.; Seguin, T. J.; Guan, Y.; Doney, A. C. *Acc. Chem. Res.* **2016**, *49*, 1061.
- (31) Sunoj, R. B. *Acc. Chem. Res.* **2016**, *49*, 1019.
- (32) The role of solvation in asymmetric catalysis has been considered through the use of explicit cluster models: Osuna, S.; Dermenci, A.; Miller, S. J.; Houk, K. N. *Chem. Eur. J.* **2013**, *19*, 14245.
- (33) Schrödinger Release 2013-3: MacroModel version 10.2. Schrödinger LLC. New York 2013.
- (34) Frisch, M. J. et al. Gaussian 09, Revision D.01 Gaussian Inc., Wallingford CT.
- (35) Jorgensen, W. L.; Chandrasekhar, J.; Madura, J. D.; Impey, R. W.; Klein, M. L. *J. Chem. Phys.* **1983**, *79*, 926.
- (36) van der Spoel, D.; van Maaren, P. J.; Coleman, C. *Bioinformatics* **2012**, *28*, 752.
- (37) Coleman, C.; van Maaren, P. J.; Hong, M.; Hub, J. S.; Costa, L. T.; van der Spoel, D. *J. Chem. Theory Comput.* **2012**, *8*, 61.
- (38) Pronk, S.; Páll, S.; Schulz, R.; Larsson, P.; Bjelkmar, P.; Apostolov, R.; Shirts, M. R.; Smith, J. C.; Kasson, P. M.; van der Spoel, D.; Hess, B.; Lindahl, E. *Bioinformatics* **2013**, *29*, 845.
- (39) Abraham, M. J.; Van Der Spoel, D.; Lindahl, E.; Hess, B. and the GROMACS development team, GROMACS User Manual version 5.1.2. <http://www.gromacs.org> 2016 (accessed 7 March 2017).
- (40) Darden, T.; York, D.; Pedersen, L. *J. Chem. Phys.* **1993**, *98*, 10089.
- (41) Parrinello, M.; Rahman, A. *J. Appl. Phys.* **1981**, *52*, 7182.
- (42) Kumar, S.; Rosenberg, J. M.; Bouzida, D.; Swendsen, R. H.; Kollman, P. A. *J. Comp. Chem.* **1992**, *13*, 1011.
- (43) Hub, J. S.; de Groot, B. L.; van der Spoel, D. *J. Chem. Theory Comput.* **2010**, *6*, 3713.
- (44) Chai, J. D.; Head-Gordon, M. *Phys. Chem. Chem. Phys.* **2008**, *10*, 6615.
- (45) Funes-Ardois, I. P., R. S. GoodVibes: GoodVibes v1.0.1, 2016, doi:<http://dx.doi.org/10.5281/zenodo.60811>. (accessed 7 March 2017).
- (46) Grimme, S. *Chem. Eur. J.* **2012**, *18*, 9955.
- (47) Marenich, A. V.; Cramer, C. J.; Truhlar, D. G. *J. Phys. Chem. B* **2009**, *113*, 6378.
- (48) Zhao, Y.; Truhlar, D. G. *Theor. Chem. Acc.* **2008**, *120*, 215.
- (49) Sickert, M.; Abels, F.; Lang, M.; Sieler, J.; Birkemeyer, C.; Schneider, C. *Chem. Eur. J.* **2010**, *16*, 2806.
- (50) Rueping, M.; Theissmann, T. *Chem. Sci.* **2010**, *1*, 473.
- (51) Johnston, R. C.; Cheong, P. H.-Y. *Org. Biomol. Chem.* **2013**, *11*, 5057.
- (52) Lum, K.; Chandler, D.; Weeks, J. D. *J. Phys. Chem. B* **1999**, *103*, 4570.
- (53) Grimme, S. *J. Comp. Chem.* **2006**, *27*, 1787.
- (54) Mardirossian, N.; Head-Gordon, M. *J. Chem. Theory Comput.* **2016**, *12*, 4303.
- (55) Seguin, T. J.; Wheeler, S. E. *Angew. Chem. Int. Ed.* **2016**, *55*, 15889.
- (56) Johnson, E. R.; Keinan, S.; Mori-Sánchez, P.; Contreras-García, J.; Cohen, A. J.; Yang, W. *J. Am. Chem. Soc.* **2010**, *132*, 6498.
- (57) Kanomata, K.; Toda, Y.; Shibata, Y.; Yamanaka, M.; Tsuzuki, S.; Gridnev, I. D.; Terada, M. *Chem. Sci.* **2014**, *5*, 3515.
- (58) Paton, R. S. *Org. Biomol. Chem.* **2014**, *12*, 1717.
- (59) Walden, D. M.; Ogba, O. M.; Johnston, R. C.; Cheong, P. H.-Y. *Acc. Chem. Res.* **2016**, *49*, 1279.
- (60) Seguin, T. J.; Wheeler, S. E. *ACS Catal.* **2016**, *6*, 2681.
- (61) Rodríguez, E.; Grayson, M. N.; Asensio, A.; Barrio, P.; Houk, K. N.; Fustero, S. *ACS Catal.* **2016**, *6*, 2506.
- (62) Steiner, T.; R. Desiraju, G. *Chem. Commun.* **1998**, 891.
- (63) Ess, D. H.; Houk, K. N. *J. Am. Chem. Soc.* **2007**, *129*, 10646.
- (64) Champagne, P. A.; Houk, K. N. *J. Am. Chem. Soc.* **2016**, *138*, 12356.
- (65) Weinhold, F. *J. Comp. Chem.* **2012**, *33*, 2363.
- (66) Raddo, P. D.; Chan, T.-H. *J. Chem. Soc., Chem. Commun.* **1983**, 16.
- (67) Meyer, O.; Ponaire, S.; Rohmer, M.; Grosdemange-Billiard, C. *Org. Lett.* **2006**, *8*, 4347.
- (68) Monaco, M. R.; Fazzi, D.; Tsuji, N.; Leutzsch, M.; Liao, S.; Thiel, W.; List, B. *J. Am. Chem. Soc.* **2016**, *138*, 14740.
- (69) Skibo, E. B.; Xing, C. *Biochemistry* **1998**, *37*, 15199.
- (70) Cytlak, T.; Saweliew, M.; Kubicki, M.; Koroniak, H. *Org. Biomol. Chem.* **2015**, *13*, 10050.
- (71) Monaco, M. R.; Prévost, S.; List, B. *Angew. Chem. Int. Ed.* **2014**, *53*, 8142.
- (72) Rueping, M.; Azap, C. *Angew. Chem. Int. Ed.* **2006**, *45*, 7832.
- (73) Li, G.; Antilla, J. C. *Org. Lett.* **2009**, *11*, 1075.

SYNOPSIS TOC (Word Style "SN_Synopsis_TOC"). If you are submitting your paper to a journal that requires a synopsis graphic and/or synopsis paragraph, see the Instructions for Authors on the journal's homepage for a description of what needs to be provided and for the size requirements of the artwork.

